Applied Surface Science 509 (2020) 144877

Contents lists available at ScienceDirect

Applied Surface Science

journal homepage: www.elsevier.com/locate/apsusc

Full Length Article

Corrosion behavior of diamond-like carbon film induced by Al/Ti co-doping

Xiaowei Xu[a,b,1], Yong Zhou[a,1], Linlin Liu[a], Peng Guo[a], Xiaowei Li[a,c,*], Kwang-Ryeol Lee[c], Ping Cui[a,b], Aiying Wang[a,d,*]

[a] Key Laboratory of Marine Materials and Related Technologies, Zhejiang Key Laboratory of Marine Materials and Protective Technologies, Ningbo Institute of Materials Technology and Engineering, Chinese Academy of Sciences, Ningbo 315201, PR China
[b] School of Physical Science and Technology, ShanghaiTech University, Shanghai 201210, PR China
[c] Computational Science Center, Korea Institute of Science and Technology, Seoul 136-791, Republic of Korea
[d] Center of Materials Science and Optoelectronics Engineering, University of Chinese Academy of Sciences, Beijing 100049, PR China

ARTICLE INFO

Keywords:
Diamond-like carbon
Co-doping
Al/Ti ratio
Corrosion behavior
Hybrid ion beam technique

ABSTRACT

Diamond-like carbon films with Al and Ti dopants (Al/Ti-DLC) were fabricated by a hybrid ion beam deposition system combined with a special design of splicing targets, in which the Al/Ti ratio was changed from 4.0 to 1.1 by tailoring the Al content. The structural evolution and corrosion behavior of Al/Ti-DLC films in 3.5 wt% NaCl solution were systematically investigated by comparing with the 316L SS and pure DLC film. Results revealed that compared with the pure DLC and 316L SS substrate, the Al/Ti-DLC film exhibited enhanced corrosion resistance by reducing the porosity and increasing the barrier for both the charge transfer and the diffusion of corrosive ions into the substrate. In particular, the anti-corrosion behavior of DLC film highly depended on the Al/Ti ratio, which decreased gradually with the Al/Ti ratio ranged from 4.0 to 1.1. Structural and EIS analysis indicated that this was ascribed to both the increased residual stress and sp^2 hybridized fraction, which induced not only the formation and propagation of cracks during the corrosion process but also the high electric conductivity and low diffusion barrier of corrosive ions, accelerating the corrosion processes at the film/substrate interface.

1. Introduction

Corrosion more or less exists in almost all metal-based systems, resulting in the significant economy and material losses every year and thus becoming a globally urgent task to develop the advanced corrosion-resistant approach for automotive, mechanical, marine, military, aerospace, and various engineering applications [1,2]. Especially for the small and key metal components, such as the mechanical arm of underwater vehicles, in order to improve their anti-corrosion capability, many methods have been adopted, including the alloying of intrinsic metals [3,4] and the effective isolation of metal with corrosive medium by introducing the organic [5,6], inorganic [7,8] or ceramic barrier layers [9]. Diamond-like carbon (DLC) film, composed of diamond and graphitic structures, exhibits excellent chemical inertness and high electrical resistivity, which is a strong candidate as protective coating to enhance the chemical stability of metal components in acid, alkali, or organic solvents [10–12].

Until now, many works have been carried out to evaluate the corrosion behavior of DLC films. For instance, Caschera et al. [13] observed that the corrosion resistance of DLC film was affected by the residual compressive stress as well as the surface and structural properties of the deposited film. Radi et al. [14] found that the stainless steel coated with DLC film presented fewer points of delamination and lower open-circuit potentials compared with the bare sample after 14 days of immersion in ethanol with different concentrations of water. Additionally, to the best of our knowledge, doping the heterogeneous atoms into intrinsic DLC structure or designing the multi-layer structure is the effective approach to improve the corrosion resistance of DLC films [15–20]. Among them, the introduction of dopants in DLC films have aroused much attention, because it can enhance the corrosion resistance, reduce the high residual stress, and raise the mechanical as well as tribological properties simultaneously. For example, Sui et al. [21] incorporated fluorine element into DLC films to improve the corrosion resistance of Ni-Ti alloys in Hank's solution. Viswanathan et al. [22] also demonstrated that Cr-DLC coatings with lower Cr contents had better corrosion resistance in 3.5 wt% NaCl solution. Dhandapani

* Corresponding authors at: Key Laboratory of Marine Materials and Related Technologies, Zhejiang Key Laboratory of Marine Materials and Protective Technologies, Ningbo Institute of Materials Technology and Engineering, Chinese Academy of Sciences, Ningbo 315201, PR China.
E-mail addresses: lixw0826@gmail.com (X. Li), aywang@nimte.ac.cn (A. Wang).
[1] These authors contributed equally to this work and should be considered as co-first authors.

https://doi.org/10.1016/j.apsusc.2019.144877
Received 5 August 2019; Received in revised form 30 October 2019; Accepted 25 November 2019
Available online 02 December 2019
0169-4332/

et al. [23] found that the corrosion resistance of DLC film was effectively improved in 3.5 wt% NaCl solution when the doped Ag content was 4.46 at.%. Zhang et al. [24] revealed that Si-doped DLC film possessed superior corrosion resistance and survived 720 h salt spray test without corrosive pitting and exfoliation yet.

Recently, based on the synergistic effects of doped metals, two or more metal elements co-doping has been taken into account, which can further polish the comprehensive property of DLC films and also convey new functions by forming the multiple nanocomposite structure. Li et al. [25] clarified that compared with pure DLC, the co-doping of Cu and Cr could significantly reduce the intrinsic residual stress by 93.6% without the serious deterioration of hardness. Sun et al. [26,27] also demonstrated that the Cu/Cr co-doped DLC films performed excellent adhesion as well as superior mechanical performance. Guo et al. [28] pointed out that the Ti/Al-DLC film exhibited both the low stress and the high hardness due to the synergistic effect of Ti and Al in amorphous carbon. Moreover, Wu et al. [29] found that in (Cu, Ce)/Ti-DLC film, Ti tended to form the titanium carbide with carbon, which blocked the corrosion path and thus improved the corrosion resistance. However, the role of co-doped metal elements on the anti-corrosion behavior of DLC in synergism is still not given much attention. The relationship between the anti-corrosion property and the structural evolution induced by the co-doped metals, especially its dependence on the ratios of co-doped metals, is not understood yet, which is requisite to shed light on the underlying corrosion mechanism and tailor the DLC structures for application.

In previous studies [28,30,31], we successfully realized the high-throughput preparation of Al/Ti co-doped DLC (Al/Ti-DLC) films with different Al/Ti ratios by the hybrid ion beam deposition system (HIB), and found that the films exhibited low residual stress, high hardness and roughness, and excellent tribological property. Hence, in the present work, a series of Al/Ti-DLC films with different ratios were also fabricated by the HIB system, in which the Al/Ti ratios were tailored by changing the doped Al content. The structural evolution and corresponding corrosion behavior induced by different Al/Ti ratios were systematically evaluated and the fundamental understanding on the anti-corrosion mechanism was explored by comparing with the intrinsic DLC and pure substrate.

2. Experimental details

2.1. Preparation of Al/Ti-DLC films

Al/Ti-DLC films were deposited on silicon P (1 0 0) wafers and 316L stainless steel (316L SS) by the HIB deposition system which was composed of a linear anode-layer ion source (ALIS) and a DC magnetron sputtering (DCMS). According to our previous study [31], the combined sputtering target, spliced by triangular Al (99.99% purity) and Ti (99.99% purity) with equal areas, was used for Al/Ti co-doping to achieve the high-throughput preparation of DLC films with different Al/Ti ratios. C_2H_2 gas was introduced into the ALIS for carbon deposition. The substrates were located between the ALIS and sputtering source, and the distance was kept at around 17.5 cm separately. Prior to deposition, the substrates were ultrasonically cleaned in acetone for 15 min and dried with nitrogen; in order to remove the existed impurities and oxides from the substrate surface and also improve the adhesive strength between the film and substrate, argon plasma was adopted to etch the sample at −100 V for about 20 min. During the deposition process, the rotation direction of substrate holder was changed every 20 min, the detailed deposition parameters were shown in Table 1, and the total deposition time was 120 min. The pure DLC film was also deposited for comparison.

2.2. Microstructure characterization

Film thickness was recorded by the surface profilometer with a shadow mask between the deposited film and bare substrate. The chemical composition and bonding state of the deposited films were analyzed by X-ray photoelectron spectroscopy (XPS, Thermo Scientific ESCALAB 250) with the monochromatic Al (mono) Kα at 160 eV incident energy. Before the measure, argon ions with the energy of 2 keV etched the film surface for 5 min to remove the impurities and contaminants. The carbon atomic bond was characterized by Raman spectroscopy (Renishaw, inVia-reflex), and the visible light with 532 nm detection laser wavelength, grating 1800 and 1% power were used. Furthermore, the cross-sectional and surface morphologies were obtained by field emission scanning electron microscope (FEI Quanta FEG250). The microstructure of Al/Ti-DLC films was acquired by high-resolution transmission electron microscopy (HR-TEM, FEI Tecnai F20).

2.3. Residual stress and electrochemical behavior tests

Residual stress tester (JLCST022, J&L Tech) was used to measure the film/substrate curvature for calculating the residual stress based on the Stoney equation. In order to evaluate the corrosion-resistant behavior of DLC films induced by Al/Ti co-doping, the electrochemical behaviors including the polarization and impedance were collected by a ModuLab (Solatron Analytical) electrochemical workstation with a three-electrode system. The counter electrode was a platinum sheet, the reference electrode was saturated Ag/(AgCl)/KCl, and the working electrode was Al/Ti-DLC film, pure DLC, and 316L SS, respectively, with an exposed area of 0.25 cm^2. The test condition was 3.5 wt% NaCl solution at room temperature. Prior to the test, the uncoated surface of all samples was polished with sandpaper to eliminate the potential effect of passivation film on the electrochemical results. The samples were immersed in 3.5 wt% NaCl solution for two hours to evaluate the open circuit potential (OCP). For the potentiodynamic polarization curve, the scanning potential ranged from −0.3 V vs. SCE to 1.5 V vs. SCE at a scanning rate of 2 mV/s. For the electrochemical impedance spectroscopy (EIS), the measured frequency changed from 10 kHz to 10 MHz and a sinusoidal disturbance voltage of 10 mV was applied. After the test, the data obtained from EIS was imported into ZSimpWin software for further fitting and analysis of the corresponding equivalent circuit.

3. Result and discussion

3.1. Composition and microstructure

Fig. 1a shows the composition of the deposited Al/Ti -DLC films, indicating that the high-throughput fabrication of DLC films is successfully achieved, in which the Ti content is fixed at 2.50 ± 0.19 at.%, while the Al content decreases from 9.21 to 2.67 at.%, corresponding to the Al/Ti ratios ranged from 4.0 to 1.1. For all Al/Ti-DLC films, the thickness is maintained at a constant value of about 1.32 ± 0.14 μm (Fig. 1b), which avoids the potential thickness-dependence of structural properties of DLC films. In addition, the cross-sectional morphologies in Fig. S1 of Supporting Information show that

Table 1
Deposition parameters for the Al/Ti-DLC films.

Sputtering current (A)	Ar flow rate (sccm)	LIS working current (A)	LIS working voltage (V)	C_2H_2 flow rate (sccm)	Bias voltage (V)	Working pressure (mTorr)
2.5	70	0.2	1100 ± 50	38	−50	4.5

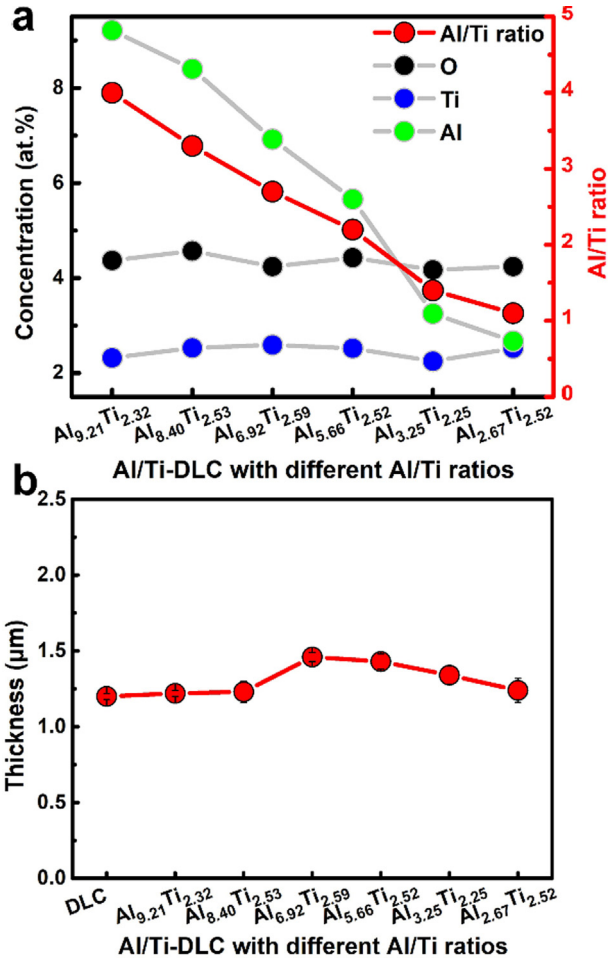

Fig. 1. (a) Composition and (b) thickness of deposited Al/Ti -DLC films.

the Al/Ti-DLC films are relatively dense and uniform, exhibiting the typical amorphous characteristics. For comparison, the pure DLC film with same thickness is also deposited, as shown in Fig. S1 of Supporting Information.

Fig. 2 shows the XPS spectra of Al/Ti-DLC films with different Al/Ti ratios, including C 1s, Ti 2p, and Al 2p, respectively. In the C 1s spectra (Fig. 2a), the major peak is located at 284.5 eV, which is a typical amorphous carbon peak. For each film, the C 1s spectrum can be deconvoluted into four small peaks, as given in Fig. 2d, corresponding to sp^3-C bond at 285.2 eV, sp^2-C bond at 284.5 eV, C-O bond at 287.5 eV, and Ti-C bond at 283 eV, respectively [29]. Moreover, the XPS spectra of Ti 2p in Fig. 2b can also be divided into four small peaks (Fig. 2e), in which a pair of major peaks, located at 455.4 eV and 461.4 eV separately, attribute to the Ti-C bond, while a pair of shoulder peaks, located at 456.8 eV and 462.6 eV separately, correspond to Ti-O bond. Combined with the C 1s analysis, these results imply that the doped Ti bonds with carbon to form the titanium carbide and TiO_x in the amorphous carbon matrix [13,31–33]. In the Al 2p spectra (Fig. 2c), a peak with the bonding energy ranged from 72 to 77 eV is observed for each case, which can be fitted into two peaks, including a main peak of Al-O bond with the binding energy of about 74 eV and a weak peak of Al-O-H bond located at about 75.3 eV [34], as shown in Fig. 2f. This indicates that the doped Al element mainly exists in the form of oxide instead of metal state in the amorphous carbon networks, owing to the presence of residual oxygen during the deposition process. In addition, with decreasing the Al/Ti ratio from 4.0 to 1.1, the reduction of Al content weakens the peak intensity of Al 2p spectra. Moreover, according to the fitting analysis of C 1s spectra (Fig. 2d), the sp^3/sp^2 ratio in each Al/Ti-DLC film is calculated as shown in Fig. S2 of Supporting Information, which decreases gradually with the Al/Ti ratio ranged from 4.0 to 1.1.

The HR-TEM micrograph and its corresponding selected area electron diffraction (SAED) diagram of Al/Ti co-doped DLC film are presented in Fig. 3. Note that in the Al/Ti-DLC film there are many nanocrystallines (black spots) existed and uniformly distributed in the network structure of amorphous carbon, but the $Al_{9.21}Ti_{2.32}$-DLC film (Fig. 3a) displays worse crystallinity and lower fraction of nanocrystallines than $Al_{2.67}$ $Ti_{2.52}$-DLC (Fig. 3b). This is also confirmed by the

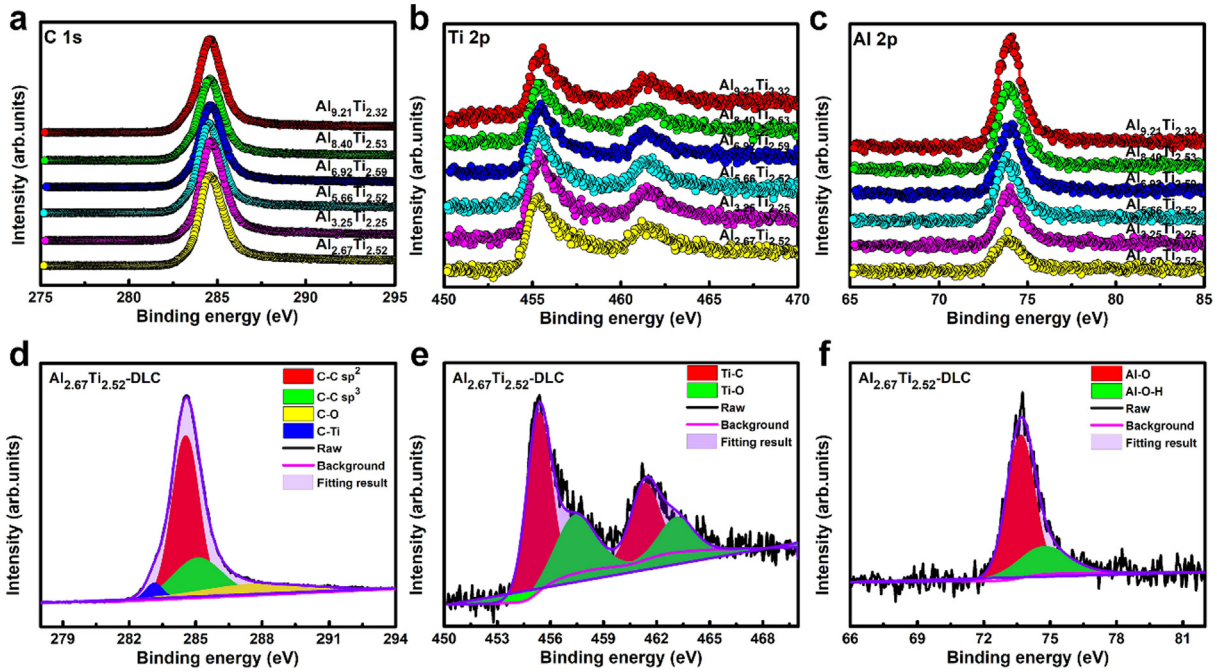

Fig. 2. XPS spectra of DLC films with different Al/Ti ratios: (a) C 1s, (b) Ti 2p, and (c) Al 2p, and the peak fitting results of (d) C 1s, (e) Ti 2p, and (f) Al 2p in $Al_{2.67}Ti_{2.52}$-DLC.

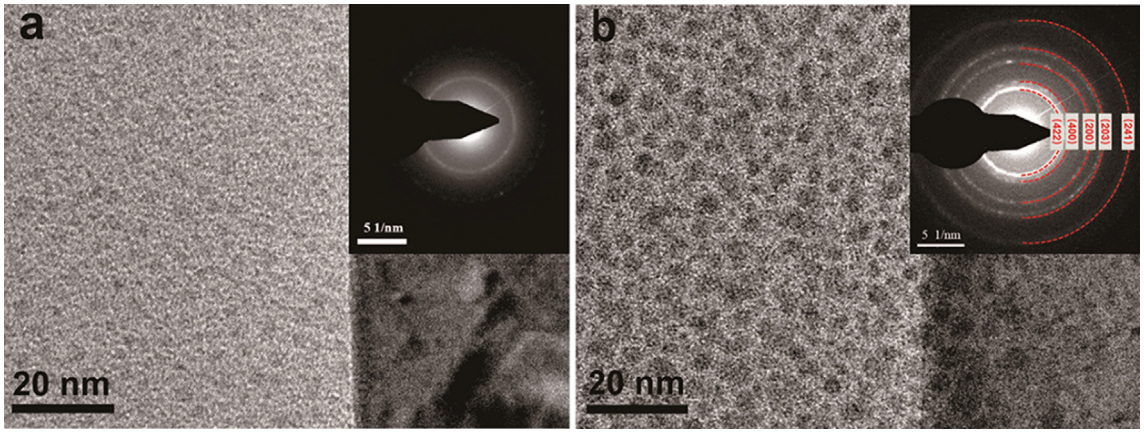

Fig. 3. HR-TEM and corresponding SAED diagrams of (a) $Al_{9.21}Ti_{2.32}$-DLC and (b) $Al_{2.67}Ti_{2.52}$-DLC film, respectively.

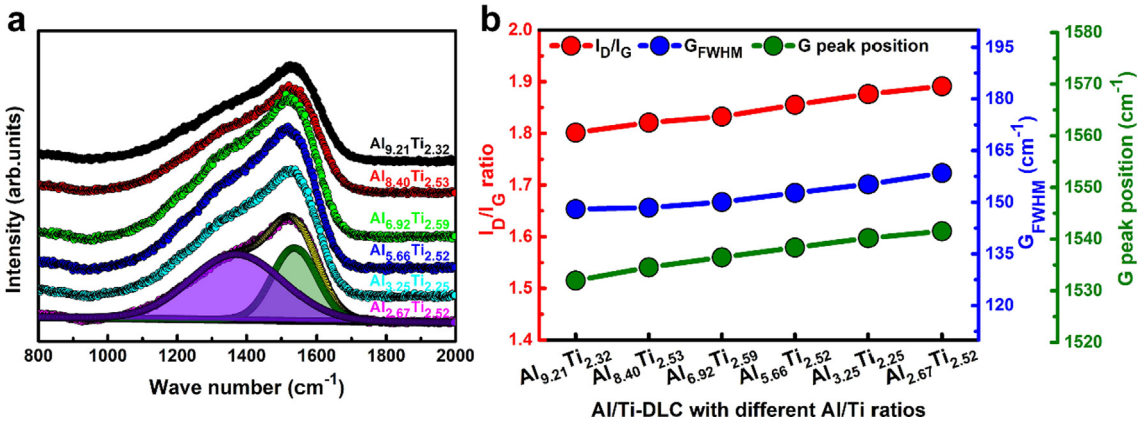

Fig. 4. (a) Raman spectra and (b) fitting results including I_D/I_G, G_{FWHM}, and G peak position of Al/Ti-DLC films with different Al/Ti ratios.

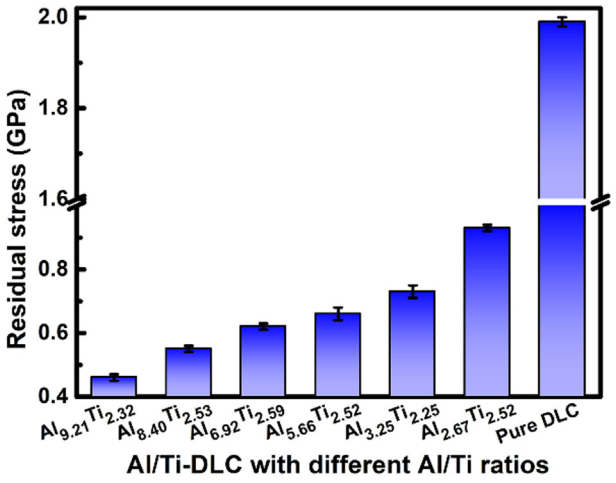

Fig. 5. Residual compressive stress of Al/Ti-DLC films as a function of Al/Ti ratio. The pre DLC is also considered for comparison.

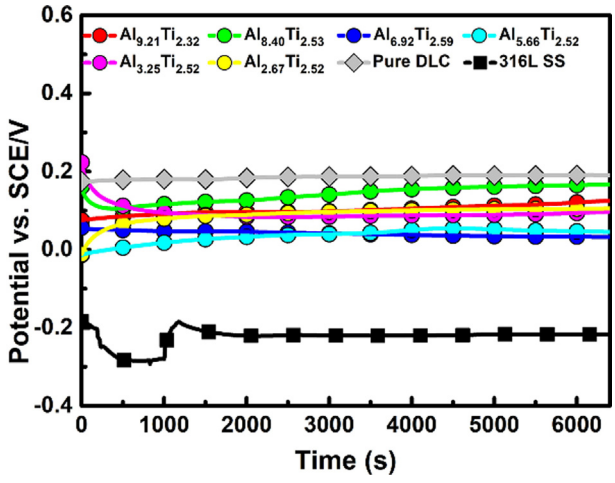

Fig. 6. Open circuit potential curves over time of Al/Ti-DLC with different doping ratios. The cases of 316L SS and pure DLC are also considered for comparison.

SAED patterns (insets of Fig. 3), in which the $Al_{9.21}Ti_{2.32}$-DLC film gives diffuse hallows, while the sharp diffraction rings are clearly observed for the $Al_{2.67}Ti_{2.52}$-DLC film, corresponding to (4 2 2), (4 0 0), and (2 2 0) reflections of cubic TiC crystallites as well as (2 2 4) and (2 0 3) reflections of tetragonal TiO_2 crystallites. Therefore, it can be deduced that with the Al/Ti ratio decreased from 4.0 to 1.1, the reduction of doped Al content is accompanied by the enhancement of crystallinity, grain size, and fraction of TiC crystallites. Previous studies [35,36] reported that in the co-doped amorphous carbon matrix, the addition of Al inhibited the formation and growth of titanium carbide grains, accounting for the structural evolution observed in the present work. This is also consistent with XPS results in Fig. 2.

Fig. 4a presents the Raman spectra of Al/Ti-DLC films with a wavelength range of 800–2000 cm^{-1} to further characterize the carbon atomic bond structure caused by different Al/Ti ratios. As well known that each Raman spectrum can be fitted into two Gaussian peaks, including D peak near 1360 cm^{-1} and G peak near 1540 cm^{-1}, in which

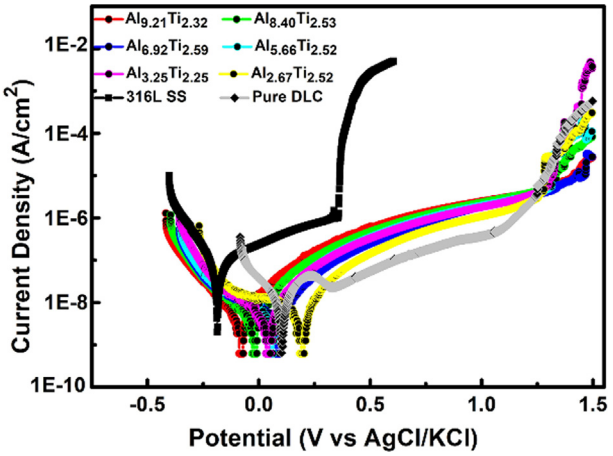

Fig. 7. Potentiodynamic polarization curves for Al/Ti-DLC with different Al/Ti ratios. The results for 316L SS and pure DLC are also considered for comparison.

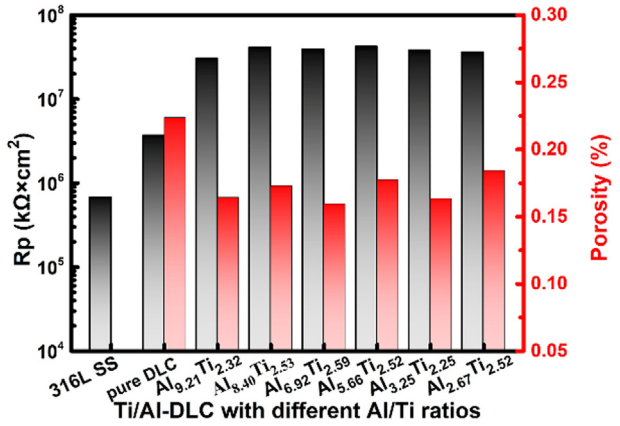

Fig. 8. Polarization resistance, R_p, and porosity for Al/Ti-DLC films with different Al/Ti ratios. The results for 316L SS and pure DLC are also considered for comparison.

the G peak originates from the stretching vibration of sp^2 carbon in both the C=C chain and aromatic ring, while the D peak is the symbol of the breathing pattern of sp^2 carbon in aromatic ring [37]. The ratio of the relative intensities of D peak and G peak (I_D/I_G) is inversely proportional to the grain size and can be used as a parameter to qualitatively estimate the hybridized structure of DLC film by combing with the deviation of G peak position. In general, the increase of G peak position and I_D/I_G ratio corresponds to a rise in sp^2 fraction [34,38]. The full width at half maximum of the G peak, G_{FWHM}, is related to the disorder degree of amorphous structure. In Fig. 4b, it can be seen that the I_D/I_G, G_{FWHM}, and G peak position all increase, indicating that with the Al/Ti ratio decreased from 4.0 to 1.1, the sp^2/sp^3 ratio and the disorder degree of the Al/Ti-DLC film increase. This attributes to the decreased Al content with Al/Ti ratio changed from 4.0 to 1.1, which facilitates the interaction between the Ti and C atoms [35,36], especially the sp^2 carbon with lower binding energy, and thus promotes the formation of sp^2 hybridized structure catalyzed by Ti atoms [22,39]. This coincides with the XPS result in Fig. S2 of Supporting Information. However, the formation and increased fraction of TiC nanocrystallines also deteriorate the intrinsic network of DLC film, leading to the disordered structure. In addition, Sui et al. [40] reported that the corrosion resistance of DLC film correlated with the sp^2/sp^3 ratio, in which the high sp^2/sp^3 ratio could result in the high conductivity following the poor corrosion resistance of the films. Therefore, the Al/Ti ratio-induced evolution of hybridized structure should be one of the important factors for the corrosion behavior of DLC film, as will be discussed later.

3.2. Residual stress of Al/Ti-DLC films

The residual compressive stress of Al/Ti-DLC films as a function of Al/Ti ratio is illustrated in Fig. 5. For comparison, the pure DLC is also considered. First, the residual stress of Al/Ti-DLC film is much smaller than that of pure DLC film (1.99 ± 0.01GPa). The reason is that the addition of Al and Ti, especially for Al without the chemical bonding with C, can play key sites to relax the distorted bond angle and length structures of carbon networks, resulting in the significant reduction of residual compressive stress, as confirmed by previous studies [28,30,41]. When the Al/Ti ratio changes from 4.0 to 1.1, the residual stress of Al/Ti-DLC film increases from 0.46 ± 0.01 to 0.93 ± 0.01 GPa monotonously, mainly attributing to the increased fraction of TiC crystallites which aggravates the disorder degree of DLC structure, as proved by the Raman analysis in Fig. 4b. It should be mentioned that the high residual stress of Al/Ti-DLC film may not only result in the easy detachment of the film from substrate, but also increase the corrosion channels in the film during the immersion process and thus accelerate the diffusion rate of corrosive ions [42].

3.3. OCP and polarization curve measurements

To elucidate the effects of different Al/Ti ratios on the corrosion performance of DLC films, the electrochemical tests are carried out in 3.5 wt% NaCl solution. Fig. 6 illustrates the variation in OCP of Al/Ti-DLC films with different Al/Ti ratios, which is widely adopted to reflect the corrosion stability of samples [30]. The cases of 316L SS and pure DLC film are also evaluated for comparison. It can be observed that the OCP values of 316L SS and pure DLC are −0.2 V and 0.2 V, respectively, while the OCP value of Al/Ti-DLC film as a function of Al/Ti ratio changes between 0.02 and 0.19 V during the whole immersion process. On the one hand, both the pure DLC and Al/Ti-DLC can significantly enhance the corrosion stability of 316L SS. On the other hand, compared with the pure DLC, the slight negative deviation in the OCP value of Al/Ti-DLC film suggests the decreased chemical stability of the surface. This is due to the doping of Al and Ti metals, activating the DLC surface and also bringing the galvanic coupling between the intrinsic carbon structure and formed TiC nanocrystalline, TiOx, and aluminum oxide phases.

In order to disclose the effect of Al/Ti co-doping on the corrosion kinetics of DLC film, Fig. 7 shows the potentiodynamic polarization curves of 316L SS, pure DLC, and Al/Ti-DLC films with different Al/Ti ratios, respectively, after immersing in 3.5 wt% NaCl solution for 1 h. Tafel fitting for these polarization curves is followed to obtain the corresponding corrosion current density (i_{corr}), corrosion potential (E_{corr}) as well as the anodic (β_a) and cathodic (β_c) Tafel slopes, as illustrated in Table 2. Note that for 316L SS, the E_{corr} is −0.19 V. After

Table 2
Summary of E_{corr}, i_{corr}, β_a, and β_c values from the fitted potentiodynamic polarization curves.

	316L SS	Pure DLC	$Al_{9.21}Ti_{2.32}$	$Al_{8.4}Ti_{2.53}$	$Al_{6.92}Ti_{2.59}$	$Al_{5.66}Ti_{2.52}$	$Al_{3.25}Ti_{2.25}$	$Al_{2.67}Ti_{2.52}$
i_{corr} (A/cm^2)	3.41E-08	2.84E-09	7.40E-10	7.05E-10	4.28E-10	6.34E-10	4.15E-10	7.04E-10
E_{corr} (V)	−0.19	0.11	−0.07	−0.01	0.09	0.07	0.05	0.20
βa (mV/dec)	140.30	43.70	100.30	91.19	64.19	57.95	53.14	56.26
βc (mV/dec)	−73.89	−53.14	−165.10	−196.30	−90.76	−163.80	−115.70	−203.90

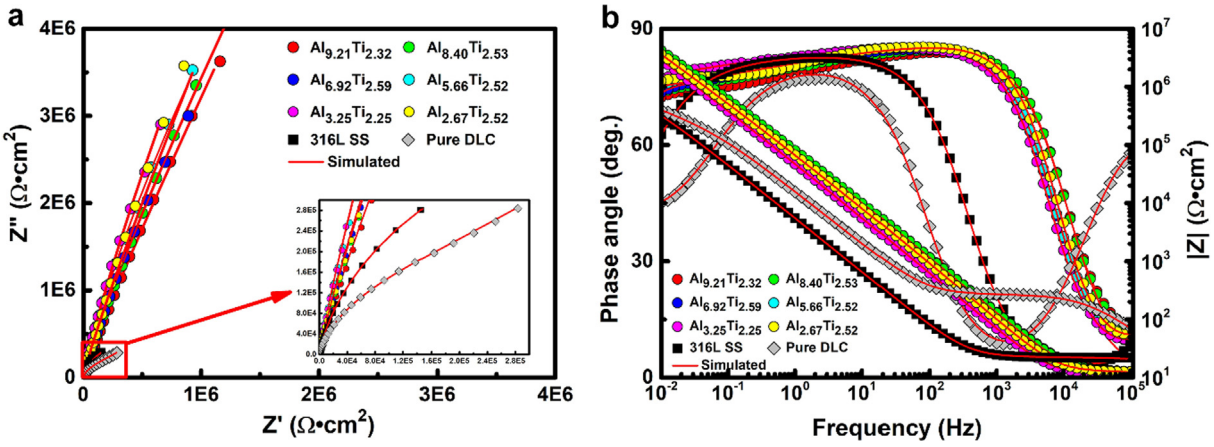

Fig. 9. EIS results for 316L SS, pure DLC, and Al/Ti-DLC films with different Al/Ti ratios after 1 h of immersion in 3.5 wt% NaCl solution. (a) Nyquist and (b) Bode diagrams, where the scatters are the experimental data plots, while the red lines are the fitting curves.

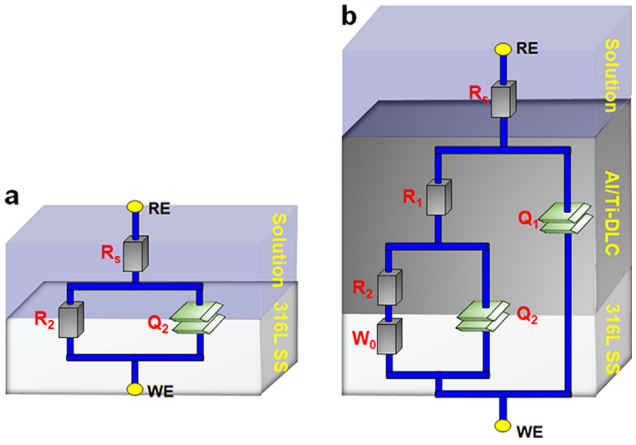

Fig. 10. EC diagrams for (a) 316L SS, (b) Al/Ti-DLC and pure DLC films after 1 h of immersion in 3.5 wt% NaCl solution.

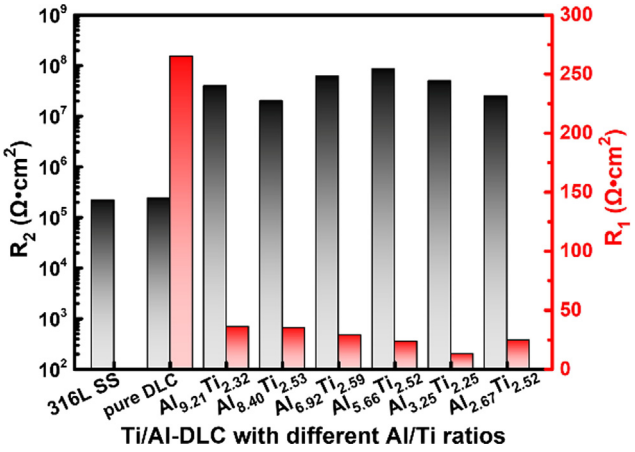

Fig. 11. Fitted R_1 and R_2 values with Al/Ti ratios in the EC model for Al/Ti-DLC films. The values for 316L SS and pure DLC are also given for comparison.

coated by the DLC or Al/Ti-DLC, the E_{corr} shifts towards the positive direction obviously, suggesting the weakened corrosion trend. Especially for the Al/Ti-DLC films, the E_{corr} value with the Al/Ti ratio ranged from 4.0 to 1.1 increases from −0.07 to 0.20 V due to the reduction of Al content with high reactivity. The i_{corr} value is normally used to reflect the corrosion rate. Compared with the 316L SS (3.41×10^{-8} A/cm^2), the i_{corr} value of pure DLC film decreases by about 10 times, but co-doping Al/Ti into DLC structure leads to the reduction of i_{corr} value by about two orders of magnitude, suggesting the best corrosion resistance of Al/Ti-DLC film combined with the change of E_{corr} value. However, there is no obvious dependence of i_{corr} value on the Al/Ti ratio observed in Table 2. In addition, for each Al/Ti-DLC film, the pitting potential is about 1.3 V (Fig. 7), which is higher than those of 316L SS (0.4 V) and pure DLC film (1.1 V), implying that the Al/Ti co-doping could more effectively inhibit the occurrence of pitting corrosion than the intrinsic DLC structure.

The difference in corrosion kinetics between the Al/Ti-DLC, pure DLC, and 316L SS is closely related with the internal defects in the films. Table 2 lists the anodic (β_a) and cathodic (β_c) Tafel slopes for both the films and bare substrate, which can be used to calculate the polarization resistance (R_p) and porosity values according to the following equations [43]:

$$R_p = \frac{\beta_a \times \beta_c}{2.33 i_{corr}(\beta_a \times \beta_c)} \quad (1)$$

$$Porosity = \frac{R_{p(sunstrate)}}{R_{p(film)}} \times 10^{-\Delta E_{corr}/\beta_{a(substsrate)}} \quad (2)$$

where the unit of R_p and i_{corr} are kΩ·cm^2 and mA/cm^2, respectively; the unit of β_a or β_c is mV/dec; $R_{p(substrate)}$ and $R_{p(film)}$ are the polarization resistances of the substrate and film separately. ΔE_{corr} is the difference of corrosion potential between the film and the bare substrate. $\beta_{a(substrate)}$ is the anodic Tafel slope for the bare substrate. The estimated values of polarization resistance and porosity are shown in Fig. 8. It can be seen that the R_p values for the pure DLC and Al/Ti-DLC films are one order and two orders of magnitude larger than that for bare 316L SS substrate, respectively, which is consistent with the results from the potentiodynamic polarization curves in Fig. 7. Furthermore, due to the co-doping of Al and Ti elements, the porosity of Al/Ti-DLC film is much lower than that of pure DLC film, implying the reduced pore defects in the films. Therefore, in Al/Ti-DLC films the high R_p value combined with the low porosity restrains the penetration of etchant solution through the film and thus reduces the generation of local corrosion, accounting for the difference in corrosion current densities between the pure DLC and Al/Ti co-doped cases (Table 2). In addition, the change of Al/Ti ratio also has little effect on the R_p and porosity values, agreeing well with the polarization curve analysis.

3.4. EIS analysis of Al/Ti-DLC films compared with pure DLC and 316L SS after 1 h of immersion in NaCl solution

Fig. 9 shows the EIS results in the form of Nyquist and Bode diagrams for 316L SS, pure DLC, and Al/Ti co-doped DLC films,

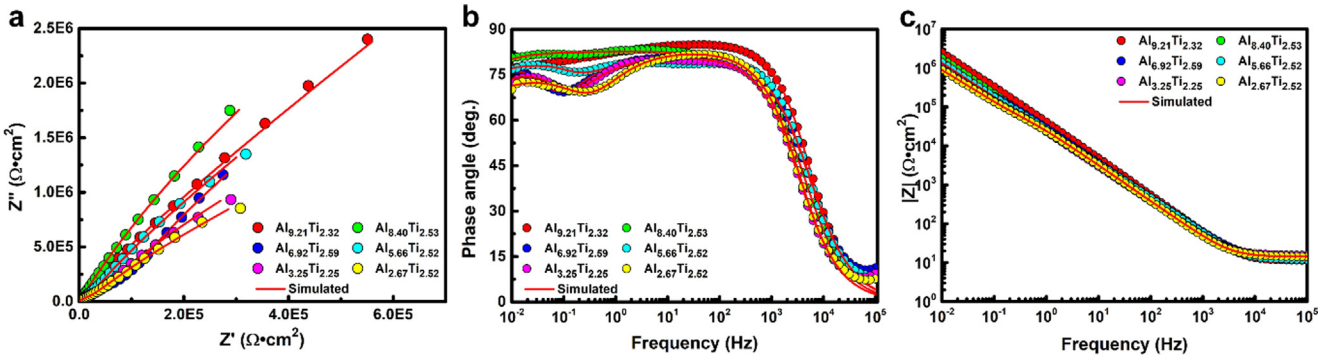

Fig. 12. EIS data for Al/Ti- DLC films with different Al/Ti ratios after 36 days immersed in 3.5 wt% NaCl solution. (a) Nyquist plots, (b) Bode phase angle diagrams, and (c) Bode impedance modulus diagram, where the scatters are the experimental data plots, while the red lines ars the fitting curves.

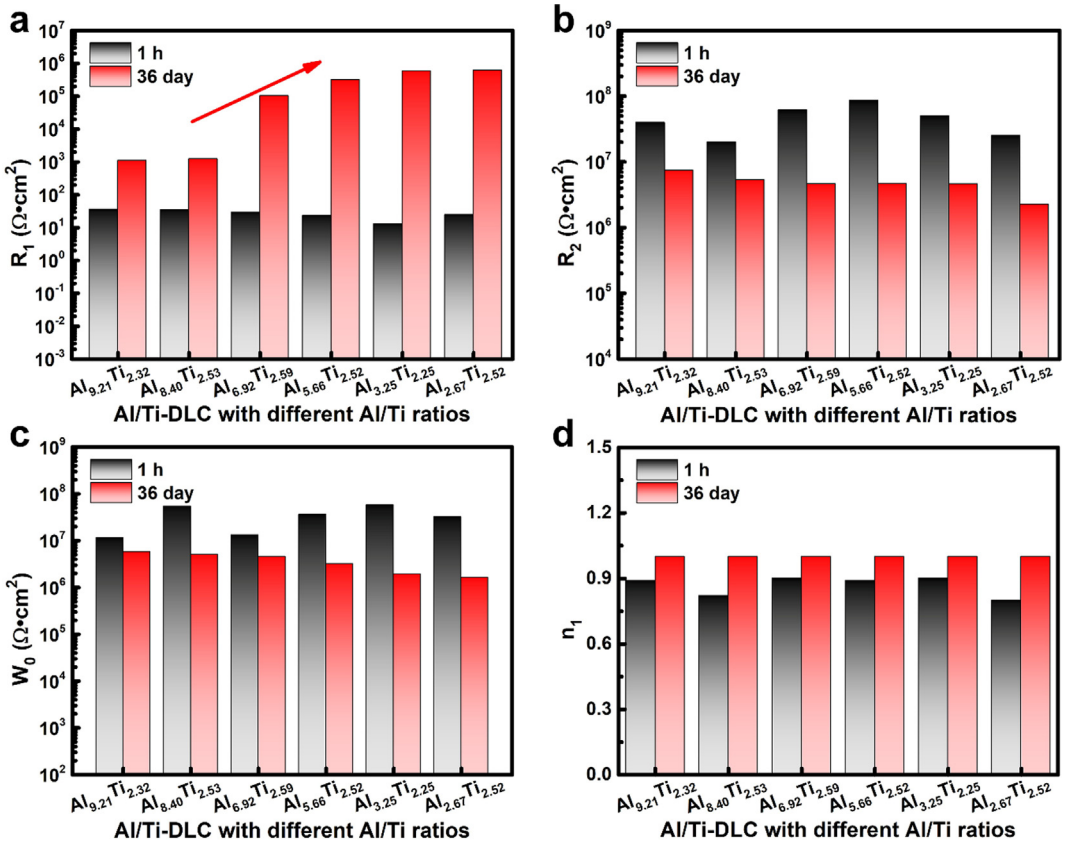

Fig. 13. Fitted parameters of EC model for the Al/Ti-DLC films with different Al/Ti ratios after 36 days immersed in 3.5 wt% NaCl solution, including (a) R_1, (b) R_2, (c) W_0, and (d) n_1. The results for the case after 1 h of immersion are also given for comparison.

respectively, after 1 h of immersion in 3.5 wt% NaCl solution. Although the total impedance value of Al/Ti-DLC film has no obvious dependence on the Al/Ti ratio (Fig. 9a and b), it is much higher than those of pure DLC and 316L SS, being consistent with the change of corrosion current density given in Table 2. In particular, the phase angle plots in Fig. 9b reveal the different time constants between the bare and DLC-coated substrates, suggesting the different corrosive behaviors. Then, the equivalent circuit (EC) fitting for EIS results in Fig. 9 is conducted for each case using the ZSimpWin software to obtain the quantitative data of each EC component and analyze the corrosion behavior.

Fig. 10a shows the EC diagram for EIS data of 316L SS with one time constant, in which R_s, Q_2, and R_2 represent the solution resistance, the capacitance of passivated film, and the charge transfer resistance in the Faraday process, respectively. However, an EC model with two time constants is deduced to describe the EIS data of both the pure DLC and Al/Ti-DLC films, as given in Fig. 10b. In this EC model (Fig. 10b), R_s also corresponds to the solution resistance; Q_1 is the capacitance of deposited films and R_1 is the pore resistance of the film due to the existed micro- and nano-defects, such as dimple, impurity and so on [44,45]; Q_2 and R_2 are the double layer capacitance of charge and corresponding charge transfer resistance generated at the interface between the films and substrate, respectively; W_0 is the Warburg impedance, corresponding to the diffusion process of corrosive medium through the micro- and nano-pores, which can be estimated as follows [46]:

$$W_0 = 1/[Y_0(j\omega)^{1/2}] \quad (3)$$

where Y_0 is a tunable parameter with a diffusion coefficient, ω is the angular frequency. It should be mentioned that due to the deviation of Q_1 and Q_2 from the ideal capacitive behavior, a constant phase component (CPE) is normally employed to replace the pure capacitance.

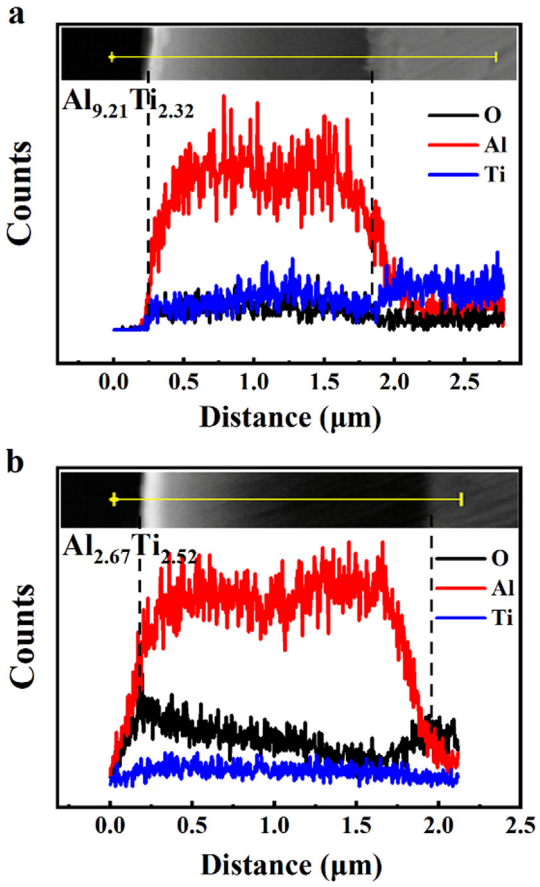

Fig. 14. Cross-sectional line scanning images of (a) $Al_{9.21}Ti_{2.32}$-DLC and (b) $Al_{2.67}Ti_{2.52}$-DLC films, respectively, after 36 days of immersion in 3.5 wt% NaCl solution.

The CPE impedance can be estimated using the following equation [46]:

$$Z_{CPE} = \frac{1}{Y_0}(j\omega)^{-n} \quad (4)$$

where n is the dispersion index, which is between 0 and 1. When n is 0, the CPE corresponds to a pure resistance; when n is 1, the CPE is regarded as an ideal capacitor, while it represents a Warburg impedance as the n is 0.5. The fitted EC parameters for each case are shown in Table S1 of Supporting Information. First, note that compared with the pure DLC film, doping Al/Ti into DLC film causes the n_1 value increased from 0.86 to 1.0, corresponding to an ideal capacitance and thus indicating the improved anti-corrosion effect on the substrate.

Fig. 11 shows of the fitted R_1 and R_2 values as a function of Al/Ti ratio in the EC model for Al/Ti-DLC films. The values for 316L SS and pure DLC are also given for comparison. It can be seen that the pure DLC film has a larger pore resistance (R_1) than Al/Ti co-doped DLC films, indicating that there are more corrosion products existed in the pores of pure DLC film due to the weak capability against corrosion. Especially, the R_2 value for Al/Ti-DLC film has slight change with Al/Ti ratio, but it is two orders of magnitude higher than that for pure DLC film. This implies that the charge transfer at the interface between the Al/Ti-DLC film and substrate is highly prohibited, contributing to the good corrosion resistance. Therefore, after 1 h of immersion in 3.5 wt% NaCl solution, the Al/Ti-DLC film exhibits much better anti-corrosion behavior than pure DLC film, but there is no obvious dependence of corrosion resistance on the Al/Ti ratio observed. However, note that although the difference in corrosion behavior between 316L SS, pure DLC, and Al/Ti-DLC can be characterized using the electrochemical analysis, there is no obvious difference observed for the corresponding morphologies before and after the corrosive tests, as shown in Fig. S3 of Supporting Information.

3.5. EIS dependence of Al/Ti-DLC films on Al/Ti ratio after 36 days of immersion in NaCl solution

Although the difference in corrosion resistance between the Al/Ti-DLC film, pure DLC, and bare 316L SS substrate can be distinguished quickly by the abovementioned analysis of polarization and EIS results, this short-term electrochemical test (only1 h of immersion in 3.5 wt% NaCl solution) provides limited information for the dependence of corrosion behavior of Al/Ti-DLC film on the Al/Ti ratio, especially its sensitivity to the Al content with relatively high reactivity. Consequently, in order to further define the role of Al/Ti ratio on the anti-corrosion ability of Al/Ti-DLC film, the long-term EIS test after 36 days of immersion in 3.5 wt% NaCl solution is evaluated. Fig. 12 shows the Nyquist and Bode diagrams for Al/Ti-DLC films with different Al/Ti ratios after 36 days immersed in 3.5 wt% NaCl solution. When the Al/Ti ratio is tailored from 4.0 to 1.1 by reducing the Al content in DLC film, the total impedance value tends to be decreased, and the Bode phase angle diagram shows two time constants for each case. By further fitting the EIS data, the EC model for Al/Ti-DLC is obtained and the fitted parameters for each EC component are listed in Table S2 of Supporting Information. Note that after the long-term immersion in the NaCl solution, the EC model for each Al/Ti-DLC film is same as the case with 1 h of immersion (Fig. 10b), although the total impedance value drops slightly for each case.

Fig. 13 shows the variation of fitted parameters of EC model with the Al/Ti ratio in the Al/Ti-DLC films after 36 days immersed in 3.5 wt % NaCl solution. The results after 1 h of immersion are also given for

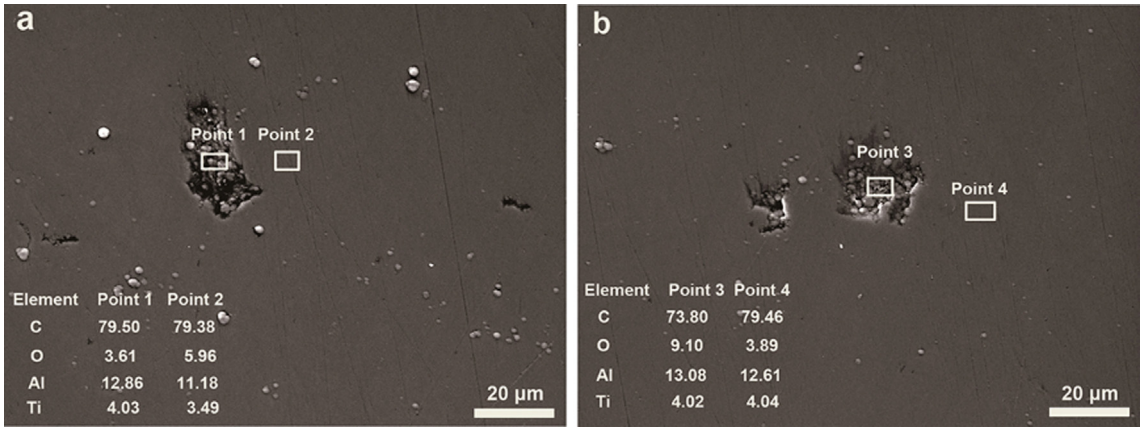

Fig. 15. Compositions of $Al_{6.92}Ti_{2.59}$-DLC film defects (a) before and (b) after 36 days of immersion in 3.5 wt% NaCl solution.

comparison. It can be seen that compared with the cases with 1 h of immersion, after the long-term immersion of Al/Ti-DLC films, the R_1 value (Fig. 13a) increases drastically, which is related with the formation of large amount of corrosion products in the micro- or nano-pores, while the R_2 (Fig. 13b), W_0 (Fig. 13c), and n_1 (Fig. 13d) values decrease obviously, suggesting the deteriorated anti-corrosion property. This is due to the enlarged porosity during the long-term immersion process, weakening the barrier of corrosive ions passing through the film and thus accelerating the corrosion and diffusion processes at the film/substrate interface. In particular, with decreasing the Al/Ti ratio from 4.0 to 1.1, both the R_2 and W_0 values drops monotonously, implying the degradation of corrosion resistance, as confirmed by the increased R_1 value in Fig. 13a. This indicates that the corrosion resistance of Al/Ti-DLC film can be enhanced by increasing the Al content, which may be affected by the reduction of residual stress, lowering the risk of the formation and propagation of cracks during the immersion process in NaCl solution [42].

The corrosion of DLC film normally occurs in the form of local corrosion (mainly pitting corrosion) and uniform corrosion. Fig. 14 presents the line cross-sectional scanning images of $Al_{9.21}Ti_{2.32}$-DLC and $Al_{2.67}Ti_{2.52}$-DLC films, respectively, after long-term immersion. As can be seen that when the film has a low Al content, there are high oxygen content existed in the film surface. The reason is that for the film with low Al content, it is followed by the high sp^2 hybridized fraction (Fig. 4), which induces the high electric conductivity and also accelerates the transportation of ions, thus resulting in the easy oxidization of film surface and the corresponding evolution of corrosion form from pitting corrosion to uniform corrosion.

In order to further explore the potential corrosion products formed in the film, Fig. 15 provides the composition of defects in the $Al_{6.92}Ti_{2.59}$-DLC film after 36 days of immersion in 3.5 wt% NaCl solution. For comparison, the result before immersion is also provided. Before the immersion process, the composition of defects is same as that of the intrinsic film, as illustrated in Fig. 15a. However, after the long-term immersion for 36 days, the aggravated oxidation is observed at the defect position with a slightly increased Al content and a constant of Ti content. This indicates that the pitting corrosion mainly occurs in the film defects, where the Al element is more easily oxidized into alumina accumulated in the pitting sites rather than dissolved in the NaCl solution [47]. Previous studies [48–50] found that the corrosion products had a filling effect on the micro-pores existed in the film. In addition, Wang et al. [51] also reported that when the SiC/DLC multilayer film was immersed in CO_2-saturated solutions, the generated corrosion products could pack the nanoscale defects and thus prevented the further corrosion of film. Therefore, increasing the Al content in Al/Ti-DLC film is favorable to generate the corrosion products of alumina, filling the pore defects and thus improving the corrosion resistance of DLC films.

4. Conclusion

In this work, the high-throughput preparation of Al/Ti-DLC films is achieved by the HIB system, in which the Al/Ti ratio changes from 4.0 to 1.1 by reducing the Al content. The corrosion resistance of Al/Ti-DLC film is evaluated by comparing with the pure DLC and bare 316L SS substrate, and the effect of Al/Ti ratio on the corrosion resistance of Al/Ti-DLC film is mainly explored. By the systematical analysis of chemical bond structure, residual stress, OCP, polarization curves, and EIS results, the main conclusions are summarized as follows:

1) In the Al/Ti-DLC films, the doped Al mainly exists in the form of oxide instead of metal state, while Ti bonds with carbon to form the titanium carbide and TiO_x in the amorphous carbon matrix.
2) As the Al/Ti ratio ranges from 4.0 to 1.1, the reduction of doped Al facilitates the interaction between the Ti and C atoms and thus promotes the increase of sp^2 hybridized structure catalyzed by Ti. However, this is not only accompanied by the enhancement of crystallinity and fraction of TiC crystallites, but also distorts the intrinsic network structure of DLC films, accounting for the increased residual stress values.
3) The results of OCP, corrosion current density, and total impedance values reveal that compared with the pure DLC and 316L SS substrate, the co-doping of Al/Ti into DLC film could highly improve the corrosion resistance due to the increased polarization resistance, the reduced film porosity, and the increased charge transfer resistance at the interface between the film and substrate, restraining the penetration of corrosive solution through the film into the substrate.
4) The long-term corrosion behavior of Al/Ti-DLC films is highly dependent on the Al/Ti ratio. EIS analysis indicates that when the Al/Ti ratio decreases from 4.0 to 1.1 by reducing the Al content, the corresponding corrosion resistance of Al/Ti-DLC film is weakened. On the one hand, this attributes to the increase of residual stress, aggravating the risk of the formation and propagation of cracks during the immersion process. On the other hand, the decrease of Al/Ti ratio is also followed by the increased sp^2 hybridized fraction, which induces the high electric conductivity, lowers the diffusion barrier of corrosive ions through the film and thus accelerates the corrosion and diffusion processes at the film/substrate interface. In addition, due to the decreased Al content, the micro- and nano-pores existed in the film could not be packed effectively, which also contributes to the reduced corrosion resistance with Al/Ti ratio from 4.0 to 1.1.
5) This work discloses the corrosion behavior of DLC films induced by Al/Ti co-doping and clarifies the fundamental mechanism, which will promote the development of DLC films with high performance for the potential application of marine key components.

Declaration of Competing Interest

The authors declared that there is no conflict of interest.

Acknowledgments

This research was supported by the National Natural Science Foundation of China (51772307), National Science and Technology Major Project (2017-VII-0012-0108), A-class pilot of the Chinese Academy of Sciences (XDA22010303), Ningbo Science and Technology Innovation Project (2018B10014), and the Korea Research Fellowship Program funded by the Ministry of Science and ICT through the National Research Foundation of Korea (2017H1D3A1A01055070).

Appendix A. Supplementary material

Supplementary data to this article can be found online at https://doi.org/10.1016/j.apsusc.2019.144877.

References

[1] S. Gkatzogiannis, J. Weinert, I. Engelhardt, P. Knoedel, T. Ummenhofer, Correlation of laboratory and real marine corrosion for the investigation of corrosion fatigue behaviour of steel components, Int. J. Fatigue 126 (2019) 90–102.
[2] M.A. Hafeez, A. Inam, M.A. Arshad, Investigation on microstructural, mechanical, and electrochemical properties of water, brine quenched and tempered low carbon steel, Mater. Res. Express 6 (2019).
[3] Y. Uematsu, T. Kakiuchi, T. Teratani, Y. Harada, K. Tokaji, Improvement of corrosion fatigue strength of magnesium alloy by multilayer diamond-like carbon coatings, Surf. Coat. Technol. 205 (2011) 2778–2784.
[4] G. Song, Recent progress in corrosion and protection of magnesium alloys, Adv. Eng. Mater. 7 (2005) 563–586.
[5] Y. Chen, X.H. Wang, J. Li, J.L. Lu, F.S. Wang, Long-term anticorrosion behaviour of polyaniline on mild Steel, Corros. Sci. 49 (2007) 3052–3063.
[6] K. Zhang, B. Xu, W. Yang, X. Yin, Y. Liu, Y. Chen, Halogen-substituted imidazoline derivatives as corrosion inhibitors for mild steel in hydrochloric acid solution, Corros. Sci. 90 (2015) 284–295.

[7] Y.X. Ou, J. Lin, S. Tong, H.L. Che, W.D. Sproul, M.K. Lei, Wear and corrosion resistance of CrN/TiN superlattice coatings deposited by a combined deep oscillation magnetron sputtering and pulsed dc magnetron sputtering, Appl. Surf. Sci. 351 (2015) 332–343.

[8] H. Yun, J. Li, H.-B. Chen, C.-J. Lin, A study on the N-, S- and Cl-modified nano-TiO_2 coatings for corrosion protection of stainless steel, Electrochim. Acta 52 (2007) 6679–6685.

[9] S.W. Jiang, L. Yang, J.N. Pang, H. Lin, Z.Q. Wang, Electrodeposition of Ni-Al_2O_3 composite coatings with combined addition of SDS and HPB surfactants, Surf. Coat. Technol. 286 (2016) 197–205.

[10] S. Khamseh, E. Alibakhshi, M. Mahdavian, M.R. Saeb, H. Vahabi, N. Kokanyan, P. Laheurte, Magnetron-sputtered copper/diamond-like carbon composite thin films with super anti-corrosion properties, Surf. Coat. Technol. 333 (2018) 148–157.

[11] G. Wu, L. Sun, W. Dai, L. Song, A. Wang, Influence of interlayers on corrosion resistance of diamond-like carbon coating on magnesium alloy, Surf. Coat. Technol. 204 (2010) 2193–2196.

[12] N. Yamauchi, K. Demizu, N. Ueda, N.K. Cuong, T. Sone, Y. Hirose, Friction and wear of DLC films on magnesium alloy, Surf. Coat. Technol. 193 (2005) 277–282.

[13] R.G. Toro, P. Calandra, B. Cortese, T. de Caro, M. Brucale, A. Mezzi, F. Federici, D. Caschera, Argon and hydrogen plasma influence on the protective properties of diamond-like carbon films as barrier coating, Surf. Interfaces 6 (2017) 60–71.

[14] P.A. Radi, A. Vieira, L. Manfroi, K.C.D.F. Nass, M.A.R. Ramos, P. Leite, G.V. Martins, J.B.F. Jofre, L. Vieira, Tribocorrosion and corrosion behavior of stainless steel coated with DLC films in ethanol with different concentrations of water, Ceram. Int. 45 (2019) 9686–9693.

[15] P. Crosasso, M. Ceruti, P. Brusa, S. Arpicco, F. Dosio, L. Cattel, Preparation, characterization and properties of sterically stabilized paclitaxel-containing liposomes, J. Control. Release 63 (2000) 19–30.

[16] A. Dorner-Reisel, C. Schürer, G. Irmer, E. Müller, Electrochemical corrosion behaviour of uncoated and DLC coated medical grade Co28Cr6Mo, Surf. Coat. Technol. 177–178 (2004) 830–837.

[17] S.C. Trippe, L. Pereira, Electrical and photocurrent analysis of Si–fluorine doped DLC films heterojunctions, Diam. Relat. Mater. 16 (2007) 1349–1352.

[18] R. Sharma, P.K. Barhai, N. Kumari, Corrosion resistant behaviour of DLC films, Thin Solid Films 516 (2008) 5397–5403.

[19] S.-S. Hadinata, M.-T. Lee, S.-J. Pan, W.-T. Tsai, C.-Y. Tai, C.-F. Shih, Electrochemical performances of diamond-like carbon coatings on carbon steel, stainless steel, and brass, Thin Solid Films 529 (2013) 412–416.

[20] S. Viswanathan, L. Mohan, P. Bera, S. Shanthiswaroop, M. Muniprakash, H.C. Barshilia, C. Anandan, Corrosion and wear resistance properties of multi-layered diamond-like carbon nanocomposite coating, Surf. Interface Anal. 50 (2018) 265–276.

[21] J.H. Sui, Z.G. Zhang, W. Cai, Surface characteristics and electrochemical corrosion behavior of fluorinated diamond-like carbon (F-DLC) films on the NiTi alloys, Nucl. Instrum. Methods Phys. Res., Sect. B 267 (2009) 2475–2479.

[22] S. Viswanathan, L. Mohan, P. Bera, V.P. Kumar, H.C. Barshilia, C. Anandan, Corrosion and Wear Behaviors of Cr-Doped Diamond-Like Carbon Coatings, J. Mater. Eng. Perform. 26 (2017) 3633–3647.

[23] V.S. Dhandapani, E. Thangavel, M. Arumugam, K.S. Shin, V. Veeraraghavan, S.Y. Yau, C. Kim, D.-E. Kim, Effect of Ag content on the microstructure, tribological and corrosion properties of amorphous carbon coatings on 316L SS, Surface Coat. Technol. 240 (2014) 128–136.

[24] M. Zhang, G. Wu, Z. Lu, L. Shang, G. Zhang, Corrosion and wear behaviors of Si-DLC films coated on inner surface of SS304 pipes by hollow cathode PECVD, Surf. Topogr. Metrol. Prop. 6 (2018).

[25] X. Li, P. Guo, L. Sun, A. Wang, P. Ke, Ab Initio Investigation on Cu/Cr Codoped Amorphous Carbon Nanocomposite Films with Giant Residual Stress Reduction, ACS Appl Mater Interfaces 7 (2015) 27878–27884.

[26] L. Sun, P. Guo, P. Ke, X. Li, A. Wang, Synergistic effect of Cu/Cr co-doping on the wettability and mechanical properties of diamond-like carbon films, Diam. Relat. Mater. 68 (2016) 1–9.

[27] L. Sun, X. Zuo, P. Guo, X. Li, P. Ke, A. Wang, Role of deposition temperature on the mechanical and tribological properties of Cu and Cr co-doped diamond-like carbon films, Thin Solid Films 678 (2019) 16–25.

[28] T. Guo, C. Kong, X. Li, P. Guo, Z. Wang, A. Wang, Microstructure and mechanical properties of Ti/Al co-doped DLC films: Dependence on sputtering current, source gas, and substrate bias, Appl. Surf. Sci. 410 (2017) 51–59.

[29] Y. Wu, S. Zhou, W. Zhao, L. Ouyang, Comparative corrosion resistance properties between (Cu, Ce)-DLC and Ti co-doped (Cu, Ce)/Ti-DLC films prepared via magnetron sputtering method, Chem. Phys. Lett. 705 (2018) 50–58.

[30] X. Li, P. Guo, L. Sun, X. Zuo, D. Zhang, P. Ke, A. Wang, Ti/Al co-doping induced residual stress reduction and bond structure evolution of amorphous carbon films: An experimental and ab initio study, Carbon 111 (2017) 467–475.

[31] Y. Zhou, P. Guo, L. Sun, L. Liu, X. Xu, W. Li, X. Li, K.-R. Lee, A. Wang, Microstructure and property evolution of diamond-like carbon films co-doped by Al and Ti with different ratios, Surf. Coat. Technol. 361 (2019) 83–90.

[32] C. Kong, P. Guo, L. Sun, Y. Zhou, Y. Liang, X. Li, P. Ke, K.-R. Lee, A. Wang, Tribological mechanism of diamond-like carbon films induced by Ti/Al co-doping, Surf. Coat. Technol. 342 (2018) 167–177.

[33] Y. Guo, P. Guo, L. Sun, X. Li, P. Ke, Q. Li, A. Wang, Tribological properties of Ti-doped diamond-like carbon coatings under dry friction and PAO oil lubrication, Surf. Interface Anal. 51 (2019) 361–370.

[34] W. Dai, J. Liu, D. Geng, P. Guo, J. Zheng, Q. Wang, Microstructure and property of diamond-like carbon films with Al and Cr co-doping deposited using a hybrid beams system, Appl. Surf. Sci. 388 (2016) 503–509.

[35] S. Zhou, L. Wang, S.C. Wang, Q. Xue, Comparative study of simplex doped nc-WC/a-C and duplex doped nc-WC/a-C(Al) nanocomposite coatings, Appl. Surf. Sci. 257 (2011) 6971–6979.

[36] S. Zhou, L. Wang, Q. Xue, Duplex doped nanocomposite carbon-based coating with self-lubricating performance, Diam. Relat. Mater. 21 (2012) 58–65.

[37] C. Casiraghi, A.C. Ferrari, J. Robertson, Raman spectroscopy of hydrogenated amorphous carbons, Phys. Rev. B 72 (2005).

[38] Y.J. Jo, T.F. Zhang, M.J. Son, K.H. Kim, Synthesis and electrochemical properties of Ti-doped DLC films by a hybrid PVD/PECVD process, Appl. Surf. Sci. 433 (2018) 1184–1191.

[39] Z. Xu, H. Sun, Y.X. Leng, X. Li, W. Yang, N. Huang, Effect of modulation periods on the microstructure and mechanical properties of DLC/TiC multilayer films deposited by filtered cathodic vacuum arc method, Appl. Surf. Sci. 328 (2015) 319–324.

[40] J.H. Sui, Z.Y. Gao, W. Cai, Z.G. Zhang, DLC films fabricated by plasma immersion ion implantation and deposition on the NiTi alloys for improving their corrosion resistance and biocompatibility, Mater. Sci. Eng., A 454–455 (2007) 472–476.

[41] X. Li, L. Li, D. Zhang, A. Wang, Ab initio study of interfacial structure transformation of amorphous carbon catalyzed by Ti Cr, and W transition layers, ACS Appl. Mater Interf. 9 (2017) 41115–41119.

[42] W. Dai, A. Wang, Deposition and properties of Al-containing diamond-like carbon films by a hybrid ion beam sources, J. Alloy. Compd. 509 (2011) 4626–4631.

[43] J. Choi, S. Nakao, J. Kim, M. Ikeyama, T. Kato, Corrosion protection of DLC coatings on magnesium alloy, Diam. Relat. Mater. 16 (2007) 1361–1364.

[44] T. Barrès, B. Tribollet, O. Stephan, H. Montigaud, M. Boinet, Y. Cohin, Characterization of the porosity of silicon nitride thin layers by Electrochemical Impedance Spectroscopy, Electrochim. Acta 227 (2017) 1–6.

[45] M. Li, Y.B. Wang, X. Zhang, Q.H. Li, Q. Liu, Y. Cheng, Y.F. Zheng, T.F. Xi, S.C. Wei, Surface characteristics and electrochemical corrosion behavior of NiTi alloy coated with IrO_2, Mater. Sci. Eng. C Mater. Biol. Appl. 33 (2013) 15–20.

[46] A. Zeng, E. Liu, I. Annergren, S. Tan, S. Zhang, P. Hing, J. Gao, EIS capacitance diagnosis of nanoporosity effect on the corrosion protection of DLC films, Diam. Relat. Mater. 11 (2002) 160–168.

[47] H.-G. Kim, S.-H. Ahn, J.-G. Kim, S.J. Park, K.-R. Lee, Effect of Si-incorporation on wear–corrosion properties of diamond-like carbon films, Thin Solid Films 482 (2005) 299–304.

[48] G. Instruments, Basics of electrochemical impedance spectroscopy, G. Instruments, Complex Imped. Corros. (2007) 1–30.

[49] B. Szczygieł, M. Kołodziej, Corrosion resistance of Ni/Al2O3coatings in NaCl solution, Trans. IMF 83 (2013) 181–187.

[50] T. Yue, J. Yu, H. Man, The effect of excimer laser surface treatment on pitting corrosion resistance of 316LS stainless steel, Surf. Coat. Technol. 137 (2001) 65–71.

[51] Z.M. Wang, J. Zhang, X. Han, Q.F. Li, Z.L. Wang, R. Wei, Corrosion and salt scale resistance of multilayered diamond-like carbon film in CO2 saturated solutions, Corros. Sci. 86 (2014) 261–267.